J|A|C|S
ARTICLES
Published on Web 07/26/2006

Photochemical Reactivity of 2-Vinylbiphenyl and 2-Vinyl-1,3-terphenyl: The Balance between Nonadiabatic and Adiabatic Photocyclization

Martial Boggio-Pasqua,[†] Michael J. Bearpark,*[,†] François Ogliaro,[‡] and Michael A. Robb*[,†]

Contribution from Imperial College London, Chemistry Department, South Kensington campus, London SW7 2AZ, United Kingdom, and Equipe de Chimie et Biochimie Théoriques, UMR 7565 − CNRS, Université Henri Poincaré, Nancy 1, 54506 Vandoeuvre-lès-Nancy, France

Received May 3, 2006; E-mail: m.bearpark@imperial.ac.uk; mike.robb@imperial.ac.uk

Abstract: A mechanism for the photochemical conversion of 2-vinyl-1,3-terphenyl to 8,9a-dihydrophenanthrene (Lewis, F. D.; Zuo, X.; Gevorgyan, V.; Rubin, M. *J. Am. Chem. Soc.* **2002**, *124*, 13664−13665) is presented in this study, based on ab initio restricted active space self-consistent field calculations and a molecular mechanics−valence bond dynamics simulation of a model system: the syn isomer of 2-vinylbiphenyl. An extended crossing seam between the ground and first excited electronic states was found to be largely responsible for the efficient photocyclization of the photochemically active syn isomer. This mechanism is nonadiabatic in nature, with an excited-state reaction pathway approaching the crossing region during the initial stage of cyclization. Dynamics simulation shows that this seam is easily accessible by vibrational motion in the branching space, once a small barrier is passed on the S_1 excited-state potential energy surface. Ultrafast radiationless decay to the ground state then follows, and the cyclization is completed on this surface. A second possible mechanism was identified, which involves complete adiabatic cyclization on the S_1 surface, with decay to the ground state (at a different conical intersection) only taking place once the product is formed. Thus, there is a competition between these two mechanisms—nonadiabatic and adiabatic—governed by the dynamics of the system. A large quantum yield is predicted for the photocyclization of the syn isomer of 2-vinylbiphenyl and 2-vinyl-1,3-terphenyl, in agreement with experimental observations.

Introduction

The aim of this work is to propose a mechanism for the photochemical conversion of 2-vinyl-1,3-terphenyl (**2o**) to 9,10-dihydrophenanthrene (**2p**). The photoisomerization of the parent compound 2-vinylbiphenyl (**1o**) was first reported by Horgan et al. in 1973.[1] They proposed a two-step mechanism: photocyclization of the open-ring reactant **1o** to yield the unstable 8a,9-dihydrophenanthrene closed-ring intermediate **1c**, which then undergoes a thermal [1,*n*] sigmatropic hydrogen shift [$n = 5$, 9, or 13] to form the observed product **1p** in both the absence and the presence of oxygen (Scheme 1). Attempts to detect 8a,9-dihydrophenanthrene intermediates from **1o** and other vinylbiphenyls under steady-state irradiation conditions were unsuccessful;[1,2] however, a short-lived transient observed by laser flash photolysis was assigned to the 10-phenyl derivative of **1c**.[3] This was the first experimental observation of such intermediate species.

More recently, Lewis et al. studied the photoisomerizations of 2-vinylbiphenyl (**1o**) and 2-vinyl-1,3-terphenyl (**2o**)[4] and a number of vinyl-substituted derivatives to study the conformational control of the photochemical behavior.[5,6] They found that the 8a,9-dihydrophenanthrene **2c** can be observed upon UV irradiation of **2o** in a rigid methylcyclohexane glass at 77 K and that 500 nm irradiation of **2c** at 77 K results in its complete reversion to **2o**. In the dark and upon warming, **2c** yields the final product **2p** via a hydrogen shift. The photocyclization of **2o**, the photochemical ring-opening of **2c** to yield **2o**, and the thermal hydrogen shift of **2c** to yield **2p** all have remarkably low activation energies. The problem with detecting the intermediate **1c** is due to the fact that the reactant **1o** exists as an equilibrium mixture of syn (*syn*-**1o**) and anti (*anti*-**1o**) rotamers: only the syn rotamer can undergo cyclization, but because of the low population of this isomer (ca. 1%) relative to the anti isomer, the photocyclization is prevented. On the other hand, 2-vinyl-1,3-terphenyl (**2o**) exists as a single rotamer (*syn*-**2o** and *anti*-**2o** are identical) as molecular symmetry enforces a syn relationship between the vinyl and ortho-phenyl groups.

[†] Imperial College London.
[‡] Université Henri Poincaré.

(1) Horgan, S. W.; Morgan, D. D.; Orchin, M. *J. Org. Chem.* **1973**, *38*, 3801−3803.
(2) op het Veld, P. H. G.; Laarhoven, W. H. *J. Chem. Soc., Perkin II* **1978**, 915−922.
(3) Fornier de Violet, P.; Bonneau, R.; Lapouyade, R.; Koussini, R.; Ware, W. R. *J. Am. Chem. Soc.* **1978**, *100*, 6683−6687.
(4) Lewis, F. D.; Zuo, X.; Gevorgyan, V.; Rubin, M. *J. Am. Chem. Soc.* **2002**, *124*, 13664−13665.
(5) Lewis, F. D.; Zuo, X. *Photochem. Photobiol. Sci.* **2003**, *2*, 1059−1066.
(6) Sajimon, M. C.; Lewis, F. D. *Photochem. Photobiol. Sci.* **2005**, *4*, 789−791.

10.1021/ja062901z CCC: $33.50

Scheme 1

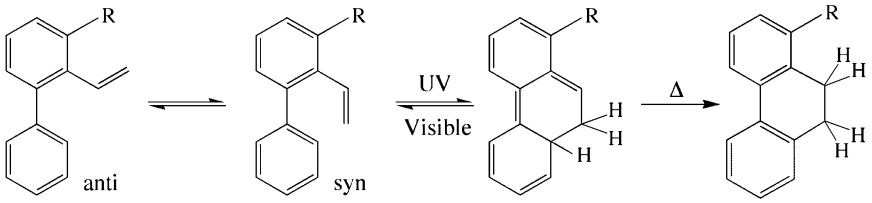

1o, R = H
2o, R = Ph

1c, R = H
2c, R = Ph

1p, R = H
2p, R = Ph

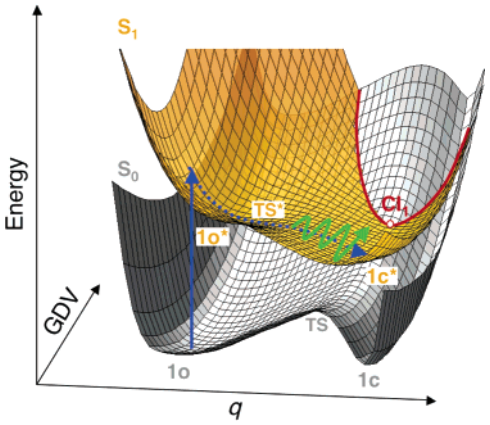

Figure 1. Schematic representation of the potential energy surfaces of 2-vinylbiphenyl based on MCSCF ab initio calculations. The two possible mechanisms for the photocyclization are illustrated: (1) nonadiabatic cyclization (green arrow) and (2) adiabatic cyclization (blue dashed arrow). *q* is the reaction coordinate, and GDV is the gradient difference vector. The red line represents the S_0/S_1 crossing seam.

Although Lewis proposed a mechanism involving an electrocyclic ring-closure of singlet **2o** and a ring-opening of singlet **2c** via a "pericyclic funnel" with small or nonexistent barriers, this funnel and the reaction path leading to it have yet to be identified. Our study focuses on determining the mechanism of the photoisomerization of 2-vinyl-1,3-terphenyl by identifying and characterizing the "pericyclic funnel" involved and the reaction pathways leading to it. Multiconfigurational self-consistent field (MCSCF) ab initio calculations were used to map out the potential energy surfaces of the ground and first excited singlet states of the 2-vinylbiphenyl (**1o**) model system. The molecular mechanics−valence bond (MMVB) hybrid method was then used to compare these two potential energy surfaces with those of 2-vinyl-1,3-terphenyl (**2o**) to ensure that the same photochemical mechanism operates in both compounds, as MCSCF calculations are too costly at present to study the larger system. MMVB was also used to run dynamics calculations, in an attempt to simulate the photocyclization and the photochemical ring-opening reactions of 2-vinylbiphenyl. The results obtained agree with the experimental observation that photocyclization of **2o** takes place via a funnel with a small barrier to overcome. However, this funnel appears as an extended crossing seam, lying in the region of the transition state on the excited state, as shown in Figure 1.

This type of extended crossing seam has now been characterized for a range of photochemical reaction mechanisms (see refs 7, 8, 9, 10, 11, and 12 for some examples), and we believe that in future it will be found for many more. A general picture is emerging, depending on a total of three coordinates (geometry changes) to be considered when describing a photochemical reaction mechanism involving a potential energy surface crossing.[13] Two of these coordinates are independent/orthogonal and make up the "branching space", which (to first order) breaks or creates the degeneracy of electronic states at an intersection point. The third coordinate is the excited state reaction path: this may be completely contained within the branching space (100% overlap), completely orthogonal (0% overlap), or anywhere in between. However, the first of these possibilities has quite different consequences from the second or third.

If an excited state reaction path is completely contained within the branching space, there are effectively only two important coordinates on this potential energy surface, and reaction path following leads to a local minimum energy point of conical intersection. Consequently, such decay points are easier to recognize and locate computationally, may be readily accessible, and will be relatively insensitive to vibrations along modes orthogonal to the reaction path. This is the case in, e.g., azulene,[14] where initial in-plane relaxation of the C−C framework on S_1 leads directly to the S_0/S_1 conical intersection responsible for ultrafast excited-state decay.

However, if the reaction path is only partially contained within or orthogonal to the branching space, following the reaction path may lead to a point of electronic state degeneracy away from a crossing minimum. This was found to be the case for the dihydroazulene to vinylheptafulvene photoisomerization, where the branching space at the crossing is made up of C−C skeletal deformations within one of the existing two rings, but the (orthogonal) excited-state reaction path involves formation of a new C−C sigma bond joining up a third ring.[7] In this case, reaction path following from excited dihydroazulene led to a surface crossing that occurred 'before' the crossing minimum, at higher energy. Alternatively, the crossing may effectively *never* be reached directly, but only indirectly via motion in the branching space, away from the reaction path. In this limiting case (as was found recently for a model diarylethylene),[8] access to the conical intersection will be controlled by the energy difference between the crossing and the reaction path, and the vibrational kinetic energy in the modes orthogonal to the reaction

(7) Boggio-Pasqua, M.; Bearpark, M. J.; Hunt, P. A.; Robb, M. A. *J. Am. Chem. Soc.* **2002**, *124*, 1456−1470.
(8) Boggio-Pasqua, M.; Ravaglia, M.; Bearpark, M. J.; Garavelli, M.; Robb, M. A. *J. Phys. Chem. A* **2003**, *107*, 11139−11152.
(9) Gómez, I.; Reguero, M.; Boggio-Pasqua, M.; Robb, M. A. *J. Am. Chem. Soc.* **2005**, *127*, 7119−7129.
(10) Paterson, M. J.; Blancafort, L.; Wilsey, S.; Robb, M. A. *J. Phys. Chem. A* **2002**, *106*, 11431−11439.
(11) Paterson, M. J.; Robb, M. A.; Blancafort, L.; DeBellis, A. D. *J. Am. Chem. Soc.* **2004**, *126*, 2912−2922.
(12) Paterson, M. J.; Robb, M. A.; Blancafort, L.; DeBellis, A. D. *J. Phys. Chem. A* **2005**, *109*, 7527−7537.
(13) Worth, G. A.; Bearpark, M. J.; Robb, M. A. In *Computational Photochemistry*; Olivucci, M., Ed.; Elsevier: Amsterdam, 2005; Vol. 16, pp 171−190.
(14) Bearpark, M. J.; Bernardi, F.; Clifford, S.; Olivucci, M.; Robb, M. A.; Smith, B. R.; Vreven, T. *J. Am. Chem. Soc.* **1996**, *118*, 169−175.

path. For these cases where the reaction path is not completely contained within the branching space, all we can say for sure is that the reaction path will not meet the crossing seam at a local minimum on the seam. We cannot know at the outset whether reaction path following will lead to the seam or not, and modeling the dynamics is crucial.

For the compounds studied here—2-vinylbiphenyl (**1o**) and 2-vinyl-1,3-terphenyl (**2o**)—there is little overlap between the S_1 reaction path (q) and the branching space of the conical S_0/S_1 intersection (represented by the single gradient difference vector, GDV) as shown in Figure 1. The conical intersection therefore appears as a line or seam as shown, suggesting that decay could occur anywhere along the adiabatic S_1 reaction path, via motion orthogonal to the reaction path, provided that the intersection seam is energetically accessible (which is more the case on part of the right-hand side of the Figure, between transition structure **TS*** and the cyclized product **c***).[7] For these systems, we did not find a point where the excited state reaction path actually meets the crossing seam. Instead, it is possible for cyclization to be completed on the excited state, followed by decay to the ground state at a different conical intersection (not shown in Figure 1). Because of the relationship between the reaction path and branching space of the conical intersection, there will be a competition between two pathways: nonadiabatic (one-step) and adiabatic followed by later decay (two-step).

For the photocyclization of 2-vinylbiphenyl (**1o**), both possible mechanisms for the photocyclization just described were identified (Figure 1). A steepest decent reaction path from the S_1 transition structure **TS*** to **1c** does not intersect the seam hyperline, which remains at higher energy. Thus, in the first mechanism, the ring closure partly takes place on the S_1 surface, the system decays via the conical intersection seam at a range of geometries between **TS*** and the minimum **1c***, and then cyclization terminates on the S_0 surface at **1c** after radiationless decay (nonadiabatic cyclization). Alternatively, complete adiabatic reaction on S_1 can yield **1c***, where the extended seam is high in energy, and decay to S_0 leading to the photoproduct must involve a different conical intersection mechanism.

Our MMVB simulations show that the photochemical ring-opening reaction cannot take place on the same potential energy surface. On the basis of multireference second-order perturbation theory (MRPT2) calculations, it appears that this process is initiated on an ionic surface, which cannot be described at the MMVB level yet.

This paper is organized as follows: the next section describes the computational methods used, followed by a section where the results are discussed. First, the potential energy surfaces of 2-vinylbiphenyl are described; these are then compared with the corresponding surfaces for 2-vinyl-1,3-terphenyl, to ensure the validity of the model. Finally, the photocyclization and photochemical ring-opening reactions are discussed, on the basis of the results of MMVB dynamics simulations.

Computational Details

MCSCF Computations. The singlet ground (S_0) and first excited (S_1) states of 2-vinylbiphenyl have been the focus of our computations, as triplet states were shown experimentally to play a minor role in the photoisomerization.[3,15] This molecule has 14 π electrons delocalized in 14 π orbitals, among which two form a sigma bond during the photocyclization process. A complete active space self-consistent field (CASSCF) calculation distributing all these electrons (14e,14o) generates nearly 6 million electron configurations, rendering the method too expensive for an extensive study of the S_0 and S_1 potential energy surfaces. (This large number of configurations cannot be reduced by symmetry because of the absence of symmetry elements in the system.) Thus, we have used the restricted active space self-consistent field (RASSCF) approach to reduce the number of configurations by restricting the excitations in the wave function. This reduction is done by subdividing the active space into three categories: a set of orbitals with a limited number of vacancies (called the RAS1 space), a fully active orbital set (RAS2), and a set of orbitals with a limited number of electrons (RAS3). We limited the excitations from the RAS1 space to singles and doubles only, and allowed only two electrons at most in RAS3. The choice of the molecular orbitals making up the different restricted active spaces is critical. The idea is to include the most important orbitals for the electron correlation in the RAS2 space, as this is where no restriction in the excitations is imposed. This strategy has proved to be very successful in reproducing the full CASSCF calculations in a recent study of another hydrocarbon (pyracylene) with 14 active electrons.[16] In the present study, we used four orbitals in RAS2, which was enough to keep our calculations accurate and cost-effective. We will denote the RASSCF calculations by the acronym RASSCF(14,9+4+9)[2,2], the figures within the brackets indicating the number of active electrons, the size of the three RAS spaces, and the excitation restrictions, respectively. In this way, the number of electron configurations was reduced by several orders of magnitude to about 34 000, a much more manageable size of configuration space. More details about how to select the orbital spaces in RASSCF can be found in ref 16 as we used a similar strategy. Full (14e,14o) CASSCF calculations were performed at selected critical points (minima and conical intersections) to assess the reliability of the RASSCF calculations. With CASSCF, full geometry optimizations were performed at minima, whereas single-point energy calculations were computed at conical intersections optimized with RASSCF.

We used a 4-31G[17a] basis set to benchmark the RASSCF calculations against CASSCF, as a larger basis set would have rendered the CASSCF calculations too costly. We then used the 6-31G* basis set,[17b,c] which includes polarization d functions on carbon atoms, to assess basis set effects on the geometries and energies at the RASSCF level. Full geometry optimizations were performed using MMVB[18] optimized structures as starting geometries. Transition states were optimized using a starting Hessian partially computed numerically along the reaction coordinate, as full frequency calculations are not feasible with such a large active space. Conical intersections were optimized using the algorithm described in ref 19. State-averaged orbitals were used, and the orbital rotation derivative correction (which is usually small) to the gradient was neglected. This gives the lowest energy point on the crossing seam, at which there are two coordinates, the gradient difference and derivative coupling vectors (branching space), which lift the degeneracy to first order. The remaining $3N-8$ coordinates (intersection space) preserve the degeneracy to first order, which therefore persists over a wide range of molecular geometries. Decay can take place away from the minimum energy point on the crossing depending on the kinetic energy of the system. A section of a crossing seam was computed by minimizing the energy difference along the gradient difference vector only, at varying geometries in the intersection space.

(15) Koussini, R.; Lapouyade, R.; Fornier de Violet, P. *J. Am. Chem. Soc.* **1978**, *100*, 6679−6683.

(16) Boggio-Pasqua, M.; Robb, M. A.; Bearpark, M. J. *J. Phys. Chem. A* **2005**, *109*, 8849−8856.

(17) (a) Ditchfield, R.; Hehre, W. J.; Pople, J. A. *J. Chem. Phys.* **1971**, *54*, 724. (b) Hehre, W. J.; Ditchfield, R.; Pople, J. A. *J. Chem. Phys.* **1972**, *56*, 2257. (c) Hariharan, P. C.; Pople, J. A. *Theor. Chim. Acta* **1973**, *28*, 213.

(18) Bernardi, F.; Olivucci, M.; Robb, M. A. *J. Am. Chem. Soc.* **1992**, *114*, 1606−1616.

(19) Bearpark, M. J.; Robb, M. A.; Schlegel, H. B. *Chem. Phys. Lett.* **1994**, *223*, 269−274.

The effect of the electron dynamic correlation was estimated using MRPT2, based on a more manageable reference (8e,8o) CASSCF/6-31G* wave function. These calculations were performed at the Franck−Condon geometries on the first two excited states.

MMVB Dynamics. The MMVB hybrid method[18] uses the molecular mechanics MM2 force field[20] to describe an inert molecular σ-framework and a parametrized Heisenberg Hamiltonian[21] to simulate CASSCF active orbitals in a valence bond space. Because of the nature of the Heisenberg Hamiltonian, MMVB cannot at present properly represent ionic states (which are dominated by charge-transfer terms) but works well for covalent excited states.[22] A full description of MMVB is given in refs 18, 23, 24, and 25. We used MMVB to compute the S_0 and S_1 potential energy surfaces of 2-vinylbiphenyl, which we benchmarked against the MCSCF computations described above. Numerical frequency calculations were performed to characterize the optimized structures obtained. Then, we computed the corresponding electronic states for 2-vinyl-1,3-terphenyl, which involves 20 π electrons delocalized in 20 π orbitals. These calculations were possible because MMVB is many orders of magnitude faster than the CASSCF method it was designed to simulate.

For the same reason, MMVB can be used to perform "on the fly" nonadiabatic dynamics.[26] The MMVB energy and gradient were used to solve the Newtonian equations of motion for 2-vinylbiphenyl. Full details of our implementation have been given elsewhere.[27] This is a "direct" dynamics method: the trajectories are propagated using a series of local quadratic approximations to the MMVB potential energy surface, as suggested by Helgaker[28] and Bakken[29] et al. The step size is determined by a trust radius. The surface-hopping algorithm of Tully and Preston[30] is used to allow excited-state trajectories to transfer to the ground state in the conical intersection region, where strong nonadiabatic coupling effects appear. The difference in energy between S_0 and S_1 at the hop is then redistributed along the component of the momentum parallel to the derivative coupling vector to ensure total energy conservation. For the simulation of the photocyclization of the syn isomer of 2-vinylbiphenyl **1o**, the trajectories were sampled in the region of a transition state **TS*** on the S_1 surface with a kinetic energy of 5 kcal/mol pointing along the ring-closure coordinate. To simulate the ring-opening reaction of **1c**, the initial S_1 geometries and velocities were sampled on the S_0 potential energy surface, using the ground-state vibrational modes.

All the MCSCF and MMVB calculations were performed using a development version of Gaussian,[31] which has been interfaced to our original MMVB code.[25] The MRPT2 calculations were computed using MOLPRO.[32]

Results and Discussion

In this section, we describe our computed potential energy surfaces and dynamics simulations. After benchmarking against CASSCF results, RASSCF calculations are shown to be sufficiently accurate to determine the potential energy surfaces of the model system 2-vinylbiphenyl (**1o**) and to provide a reference set of geometries and energies. MMVB was then used to compute the same potential surfaces and compared with RASSCF, showing that MMVB in turn is accurate enough to compute the potential surfaces of 2-vinyl-1,3-terphenyl (**2o**)—for which RASSCF/CASSCF is too expensive at present—and to undertake a dynamics study.

Potential Energy Surfaces of 2-Vinylbiphenyl. The RASSCF potential energy profile for the S_0 and S_1 states of the parent compound 2-vinylbiphenyl (**1o**) is presented in Figure 2. The energies from which this profile is derived are collected in Table 1.

Figure 2 shows that the open-ring isomer **1o** is more stable that the closed-ring isomer **1c** by ca. 28 kcal/mol on the ground-state surface. The barrier to overcome for a thermal cyclization of **1o** (via **TS**) is over 60 kcal/mol. Interestingly, the barrier for cyclization is about 10 times smaller on the S_1 surface, the transition state **TS*** being only 6 kcal/mol above the S_1 open-ring minimum **1o***. Also, as opposed to the ground-state topology, the closed-ring isomer **1c*** is lower in energy than the open-ring isomer **1o*** (by 16 kcal/mol) on the S_1 surface.

Two distinct S_0/S_1 conical intersection minima (**CI_1** and **CI_2**) are indicated in Figure 2. They both display three weakly coupled π electrons, a type of conical intersection that has been repeatedly documented.[33,34,35] Their structures are shown in Figure 3 and are characterized by an isosceles triangular configuration of the three coupled electrons, accompanied by a "kink". The two coordinates that lift the degeneracy (the branching space) at **CI_1** are shown in Figure 4. **CI_1** is particularly interesting, because one of the two branching space coordinates here (the derivative coupling vector, DCV) involves the new C−C bond breaking/forming process: the reaction coordinate. The most important feature of this CI is therefore that the reaction path lies partly in the branching space, and the conical intersection appears as a crossing seam nearly parallel to the reaction coordinate *q*. To verify this, we have computed a section of the crossing seam along the coordinate *q*, which is represented in Figure 2 as the red dotted line. The consequence of this topology is that access to the crossing seam depends on vibrational motion inside the branching space, as shown by the dynamics simulations (see below). More precisely, Figure 5 shows that the reaction path overlaps with the derivative coupling vector (angle of approximately 70°), whereas it is orthogonal to the gradient difference vector. Therefore, following the reaction path will bring the system in the vicinity of the crossing seam, where the two highlighted carbon atoms in Figure 5 are approaching each other. Then, vibration along the gradient difference vector is needed for the system to reach the intersection seam (i.e., for bringing the system into an isosceles triangular conformation required for the degeneracy). Similar

(20) Allinger, N. L. *Adv. Phys. Org. Chem.* **1976**, *13*, 1−85.
(21) (a) Anderson, P. W. *Phys. Rev.* **1959**, *115*, 2−13. (b) Said, M.; Maynau, D.; Malrieu, J.-P.; Bach, M.-A. G. *J. Am. Chem. Soc.* **1984**, *106*, 571−579. (c) Said, M.; Maynau, D.; Malrieu, J.-P. *J. Am. Chem. Soc.* **1984**, *106*, 580−587. (d) Durand, P.; Malrieu, J.-P. *Adv. Chem. Phys.* **1987**, *67*, 321−412.
(22) Bearpark, M. J.; Bernardi, F.; Olivucci, M.; Robb, M. A. *J. Phys. Chem. A* **1997**, *101*, 8395−8401.
(23) Bearpark, M. J.; Robb, M. A.; Bernardi, F.; Olivucci, M. *Chem. Phys. Lett.* **1994**, *217*, 513−519.
(24) Bearpark, M. J.; Boggio-Pasqua, M. *Theor. Chem. Acc.* **2003**, *110*, 105−114.
(25) Bearpark, M. J.; Boggio-Pasqua, M.; Robb, M. A.; Ogliaro, F. *Theor. Chem. Acc.* **2006**, available on-line (DOI: 10.1007/s00214-006-0113-5).
(26) Klein, S.; Bearpark, M. J.; Smith, B. R.; Robb, M. A.; Olivucci, M.; Bernardi, F. *Chem. Phys. Lett.* **1998**, *292*, 259−266.
(27) Bearpark, M. J.; Robb, M. A.; Smith, B. R.; Bernardi, F.; Olivucci, M. *Chem. Phys. Lett.* **1995**, *242*, 27−32.
(28) Helgaker, T.; Uggerud, E.; Jensen, H. J. A. *Chem. Phys. Lett.* **1990**, *173*, 145−150.
(29) Bakken, V.; Millam, J. M.; Schlegel, H. B. *J. Chem. Phys.* **1999**, *111*, 8773−8777.
(30) (a) Tully, J. C.; Preston, R. K. *J. Chem. Phys.* **1971**, *55*, 562−572. (b) Tully, J. C. In *Dynamics of Molecular Collisions*; Miller, W. H., Ed.; Plenum Press: New York, 1976; part B, p 217.
(31) Frisch, M. J.; et al. *Gaussian Development Version*, revision B.07; Gaussian, Inc.: Pittsburgh, PA, 2003.
(32) Werner, H.-J.; et al. *MOLPRO*, version 2002.6; Birmingham, UK, 2003.
(33) Celani, P.; Garavelli, M.; Ottani, S.; Bernardi, F.; Robb, M. A.; Olivucci, M. *J. Am. Chem. Soc.* **1995**, *117*, 11584−11585.
(34) Bernardi, F.; Olivucci, M.; Robb, M. A. *Isr. J. Chem.* **1993**, *33*, 265−276.
(35) Garavelli, M.; Smith, B. R.; Bearpark, M. J.; Bernardi, F.; Olivucci, M.; Robb, M. A. *J. Am. Chem. Soc.* **2000**, *122*, 5568−5581.

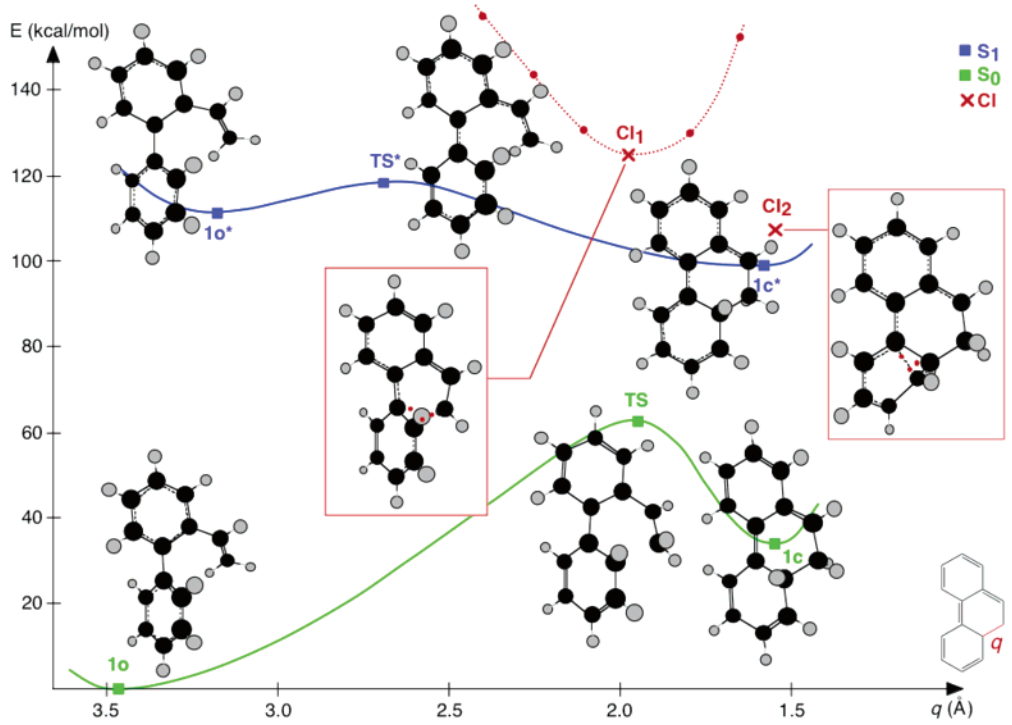

Figure 2. Potential energy profile of 2-vinylbiphenyl obtained at the RASSCF(14,5+4+5)[2,2]/6-31G* level of calculation. Conical intersections (CI) are represented in red. *q* is the ring-closure reaction coordinate.

Table 1. RASSCF(14,5+4+5)[2,2]/6-31G* Energies for 2-Vinylbiphenyl (Open-Ring, **1o**)/8a,9-Dihydrophenanthrene (Closed-Ring, **1c**)[a]

geometry	S_0[b]	S_1[b]	q[c]	ΔE ($S_1 - S_0$)[d]	ΔE (S_0)[d]	ΔE (S_1)[d]
syn-**1o**	−537.28426	−537.09015	3.476	121.8	0.0	
TS	−537.18680	−537.06282	1.960	77.8	61.2	
1c	−537.23893	−537.09818	1.547	88.3	28.4	
syn-**1o***	−537.25692	−537.10896	3.200	92.8		0.0
TS*	−537.20146	−537.09946	2.736	64.0		6.0
1c*	−537.21903	−537.13444	1.569	53.1		−16.0
$\mathbf{CI_1}$[e]	−537.08904	−537.08894	1.973	< 0.1		12.6
$\mathbf{CI_2}$[e]	−537.12486	−537.12484	1.550	< 0.1		−10.0
$\mathbf{CI_3}$[e]	−537.08472	−537.08461	3.216	< 0.1		15.3

[a] See Table S1 for results in a 4-31G basis set. [b] Electronic S_0 and S_1 energies in hartrees. [c] *q* is the bond length in Å of the C−C bond breaking/forming. [d] Energy differences (ΔE) in kcal/mol. $\Delta E(S_n)$ are the relative energies of state S_n at the geometry specified in the first column, with the open-ring S_n minimum energy as reference. [e] Conical intersections (CI) have been optimized using state-averaged orbitals.

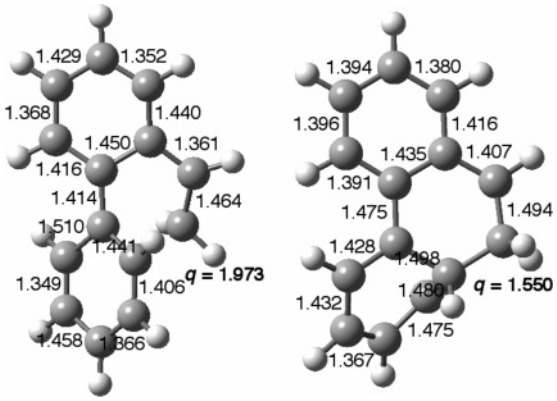

Figure 3. The structures of the conical intersection minima $\mathbf{CI_1}$ (left) and $\mathbf{CI_2}$ (right), shown in Figure 2. *q* is the bond length of the new C−C bond formed during cyclization. All bond lengths are in Å.

behavior has now been encountered in a number of studies[7−9] and appears to be more general than previously thought.

The second crossing ($\mathbf{CI_2}$) involves a prefulvene-like conical intersection,[36] lying only 6 kcal/mol above the **1c*** minimum. Both of these crossings are involved in the dynamics simulation presented in the last two sections but play different roles. $\mathbf{CI_1}$ is the seam responsible for product formation in a nonadiabatic cyclization process, whereas $\mathbf{CI_2}$ is involved in the radiationless decay to the ground state after adiabatic cyclization has been completed on the S_1 surface and plays a role as a photophysical decay channel for **1c**.

CASSCF(14,14)/4-31G calculations were performed to assess the reliability of the RASSCF computations. The results are collected in Table 2. Comparison with the RASSCF results obtained with the same basis set (see Table S1) shows that RASSCF reliably reproduces the CASSCF energetics. The main difference concerns the relative energy of the CIs. $\mathbf{CI_1}$ and $\mathbf{CI_2}$ are higher in energy relative to **1o*** at the CASSCF level, but this is partly due to the fact that the conical intersections were not reoptimized. Minima and transition structures were reoptimized with CASSCF, however, and Figure S1 shows there were no significant changes in geometry. Thus, RASSCF can be used as an alternative to CASSCF, which is computationally too demanding for an extensive study of this system at present.

The results of the MMVB calculations are collected as Supporting Information in Figures S2 and S3 and in Table S2. All the critical points (minima, transition states, and CIs) located with RASSCF have been found with MMVB (Figure S3).

Overall, the MMVB potential energy profile is similar to the RASSCF one (Figure 6): large potential energy barrier on the

(36) Palmer, I. J.; Ragazos, I. N.; Bernardi, F.; Olivucci, M.; Robb, M. A. *J. Am. Chem. Soc.* **1993**, *115*, 673−682.

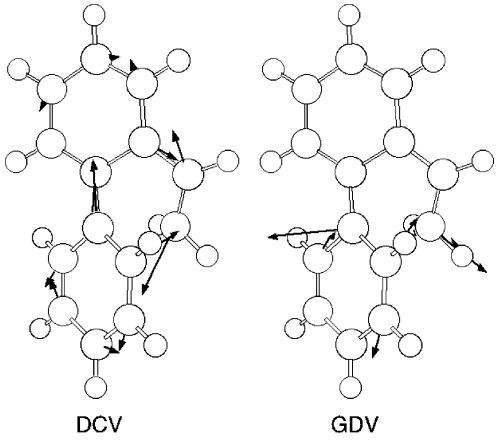

Figure 4. Derivative coupling (DCV) and gradient difference (GDV) vectors at **CI_1**.

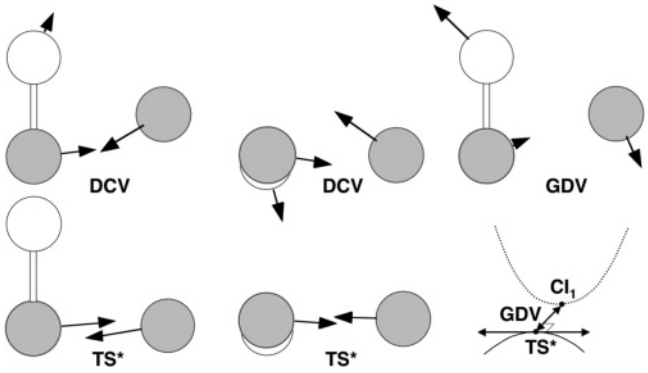

Figure 5. Comparison of the branching space (DCV, GDV) at **CI_1** and the reaction coordinate at **TS***. Side views (middle pictures) show the angle between the reaction coordinate and the derivative coupling vector (DCV). The reaction path lies only partially in the branching space, and vibration in the orthogonal gradient difference vector (GDV) is needed to bring the system to the intersection seam.

Table 2. CASSCF(14,14)/4-31G Energetics for 2-Vinylbiphenyl (Open-Ring, **1o**)/8a,9-Dihydrophenanthrene (Closed-Ring, **1c**)

geometry	S_0[a]	S_1[a]	q[b]	ΔE (S_1-S_0)[c]	ΔE (S_0)[c]	ΔE (S_1)[c]
syn-**1o**	−536. 55143	−536.37265	3.457	112.2	0.0	
TS	−536.45184	−536.33965	1.964	70.4	62.5	
1c	−536. 49681	−536.36750	1.561	81.1	34.3	
syn-**1o***	−536.53433	−536. 38550	3.206	93.4		0.0
TS*	−536.46822	−536.37404	2.638	59.1		7.2
1c*	−536.47927	−536. 39892	1.586	50.4		−8.4
CI_1[d]	−536.35822	−536.35347	1.979	3.0		20.1
CI_2[d]	−536.38048	−536.38015	1.553	0.2		3.4

[a] Electronic S_0 and S_1 energies in hartrees. [b] q is the bond length in Å of the C−C bond breaking/forming. [c] Energy differences (ΔE) in kcal/mol. $\Delta E(S_n)$ are the relative energies of state S_n at the geometry specified in the first column, with the open-ring S_n minimum energy as reference. [d] Energies computed at RASSCF(14,5+4+5)[2,2]/4-31G optimized geometries, using state-averaged orbitals.

ground-state surface between **1o** and **1c**; small potential energy barrier for the cyclization on the S_1 surface; two conical intersections involving the same three weakly coupled electrons. Nonetheless, there are some differences in detail. With MMVB, the closed-ring isomer **1c** is more stable than the open form **1o** by ca. 14 kcal/mol, whereas **1o** is the more stable by 34 kcal/mol at the CASSCF level. Similarly, **1c*** is 33 kcal/mol below **1o*** at the MMVB level, against only 8 kcal/mol at the CASSCF level. MMVB therefore tends to overstabilize the closed-ring structures relative to the open-ring ones. The two conical intersections, **CI_1** and **CI_2**, are also found lower in energy relative to the excited-state minima.

From a structural point of view, there are two main differences between the MMVB and MCSCF results. First, both open-ring minima (**1o** and **1o***) have the two phenyl rings orthogonal to each other with MMVB: the dihedral angle linking the two rings is 94°, whereas it is 64 and 39° for **1o** and **1o***, respectively, with CASSCF. This is probably due to a deficiency in the MMVB parametrization. Moreover, the flat MMVB profile on the S_1 surface involves several additional local minima (**1a*** and **1b***) and transition states (**TS_a*** and **TS_b***), shown in Figure S4. The main transition state concerning the cyclization **TS*** is encountered much "later" than the one at the MCSCF level: the bond length q of the C−C bond involved in the cyclization is equal to 1.95 Å, against 2.64 Å at the CASSCF level. With CASSCF, it appears that the **TS*** barrier has to be overcome for any radiationless decay to occur, whereas in MMVB we find **TS*** near to but after **CI_1**, along the coordinate shown in Figure 6. However, such transition states may not be well defined, as frequency calculations were not feasible with CASSCF or RASSCF. The consequences of these differences on the dynamics will be discussed in the next sections, but as we shall see, the overall mechanism for the photocyclization of 2-vinylbiphenyl can still be described using the MMVB potential.

Potential Energy Surfaces of 2-Vinyl-1,3-terphenyl. To ensure 2-vinylbiphenyl (**1o**) is a good model system for describing the photocyclization of 2-vinyl-1,3-terphenyl (**2o**), we need to compare the potential energy profiles of the two systems. Because of the large size of **2**, the S_0 and S_1 potential energy profiles have been computed with MMVB only. The results are shown in the Supporting Information (Figure S5/Table S3); the main point is that the potential energy profiles remain similar to those found for **1**, as shown in Figure 6. However, the potential energy barrier for cyclization on the S_1 surface is effectively canceled for **2**. This means that the cyclization is virtually barrierless in 2-vinyl-1,3-terphenyl, and because of this and the fact that there is only a single active rotamer, the cyclization of 2-vinyl-1,3-terphenyl is easier than that of 2-vinylbiphenyl. Note the existence of analogous conical intersections **CI_1** and **CI_2** in **1** and **2**, providing matching funnels for internal conversion to the ground state. We therefore conclude that the syn rotamer of 2-vinylbiphenyl is a good model system for describing the photocyclization of 2-vinyl-1,3-terphenyl.

Photocyclization of 2-Vinylbiphenyl. As discussed earlier, the photocyclization of 2-vinylbiphenyl itself cannot be observed experimentally because of the low population of the syn rotamer (1%) compared with the unreactive anti rotamer (99%). This has led Lewis and co-workers[4] to study the photochemical behavior of 2-vinyl-1,3-terphenyl, which exists as a single syn rotamer. Nonetheless, as we have just shown using MMVB calculations, 2-vinylbiphenyl **1o** is a good model system to use to describe the mechanism of the photocyclization of 2-vinyl-1,3-terphenyl **2o**.

The *anti*-**1o** rotamer lies about 2 kcal/mol below the *syn*-**1o** rotamer (Table S2) with an anti-to-syn barrier of 6.2 kcal/mol.

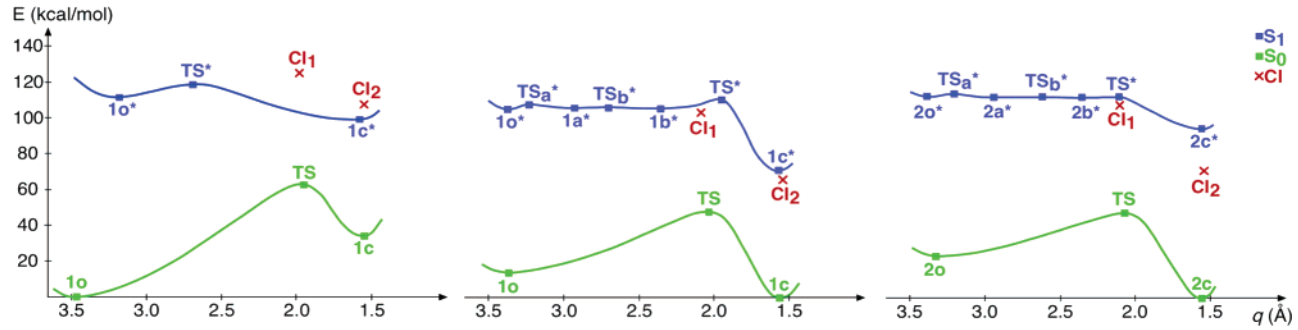

Figure 6. Potential energy profiles for 2-vinylbiphenyl with RASSCF (left), MMVB (center), and 2-vinyl-1,3-terphenyl with MMVB (right).

On the S_1 surface, *anti*-**1o*** is also 2 kcal/mol lower in energy than *syn*-**1o*** but the isomerization barrier has increased to 8.1 kcal/mol. This effect is even more pronounced at RASSCF level where no barrier was found on S_0 and a barrier of 12.2 kcal/mol appears on S_1 (Table S1). This explains why *anti*-**1o** itself is photostable, as the isomerization to the syn rotamer is even more difficult on the S_1 surface.

At this stage, we assume that the dynamics takes place on the S_1 electronic state. This follows from MRPT2 calculations performed at the Franck−Condon geometry **1o**, which show that the lowest excited state is the covalent L_b state (HOMO−1 → LUMO, HOMO → LUMO+1) in agreement with MCSCF results, whereas the ionic L_a state (HOMO → LUMO) lies 6 kcal/mol above. As explained in the previous section, there are still two problems in the description of the S_1 surface of **1** with MMVB: the erroneous torsion angle between the two phenyl rings in syn-**1o*** and the poor description of the transition state region **TS***. Because of the small photoisomerization barrier to overcome, the usual procedure for simulating dynamics is to start the trajectories in the region of the transition state, rather than the minimum. (An attempt to sample trajectories from *syn*-**1o** led to the system oscillating in the *syn*-**1o*** minimum without overcoming the **TS_a*** transition state). On the other hand, starting trajectories from **TS*** would be problematic, as the position of the transition state on the S_1 potential energy profile is inaccurate. We therefore decided to start the trajectories in the region of **TS_b***, a transition state that looks much more like the **TS*** found at the MCSCF level. The transition vectors corresponding to **TS_b*** and **TS*** are very similar and correspond to the ring-closure coordinate, whereas the transition vector of **TS_a*** correspond to the twist between the two phenyl rings (Figure S7).

The results of the trajectories simulating the photocyclization of *syn*-**1o** are collected in Table 3. Figure 1 illustrates the two mechanisms emerging from this simulation. In the first, the system undergoes an internal conversion at **CI_1** and the cyclization takes place subsequently on the S_0 surface. In the second, the cyclization occurs adiabatically on the S_1 surface, which is followed by an internal conversion at **CI_2**. The second mechanism was only observed in one trajectory (trajectory no. 6); in all the others, the system decays at the **CI_1** crossing seam. The **CI_1** intersection seam is accessible by vibrational motion along GDV. This is due to the existence of an extended crossing seam near parallel to the reaction coordinate. The degeneracy is preserved for a wide range of geometries, as the reaction coordinate is partially included in the branching space. Thus, radiationless decay to the ground state can take place at various

Table 3. MMVB Dynamics Simulation for the Photocyclization of 2-Vinylbiphenyl **1o**

trajectory[a]	ΔE_{ic}[b]	q (Å)[c]	t_{hop} (fs)[d]	t_{end} (fs)[e]	product
0	0.7	2.117	307	535	**1c**
1	62.1	2.118	145	564	**1c**
2	61.8	2.244	745	924	**1c**
3	51.9	2.087	173	210	**1o**
4	60.0	2.082	727	756	**1o**
5	65.4	2.077	714	1442	**1c**
6	49.7	1.559	432	484	**1c**
7	56.7	2.179	221	1010	**1c**
8	64.0	2.048	216	1059	**1c**
9	56.8	2.057	179	1328	**1c**
10	56.7	2.093	177	987	**1c**

[a] Trajectory 0 was obtained with 5 kcal/mol along transition mode of **TS_b***. Other trajectories have 5 kcal/mol along transition mode and other vibrational modes are sampled from the ground vibrational level of **TS_b***. [b] Energy difference in kcal/mol between the energy at which internal conversion occurs and the energy minimum at **1o***. [c] q is the bond length in Å of the C−C bond breaking/forming at the hop. [d] Time at the radiationless decay. [e] Total time of the trajectory.

geometries along the seam depending on vibrational motion along GDV. A similar mechanism was found in the photochromism of diarylethenes, for which a detailed discussion of the concept of extended crossing seam and the consequences on the dynamics is given.[8] In the present trajectories, the system oscillates for a short time (a few hundreds of fs) in the local minimum **1b*** before reaching the seam. Radiationless decay to the ground state follows and the system can either relax back to the **1o** minimum or form the new photoproduct **1c**. In this case, the cyclization is completed on the S_0 surface. For trajectory no. 6, the system overcomes the barrier **TS*** and misses the crossing seam **CI_1**. The cyclization takes place adiabatically on S_1 and the system reaches the **1c*** minimum. Then, internal conversion at **CI_2** follows, as the crossing is easily accessible from this minimum (see next subsection), and decay to S_0 leads to the photoproduct **1c**. The results of this small batch of trajectories seem to indicate that the formation of the photoproduct **1c** is favored over the regeneration of **1o** (branching ratio $\approx$ 4.5). This could be due to inertial reasons, as the flow of energy is directed along the cyclization coordinate. This is in agreement with experimental results as the quantum yield for the ultimate formation of **2p** is 0.87, providing an upper bound of 0.13 for the quantum yield of return to the ground state of **2o** via the funnel **CI_1** (branching ratio = 6.7).[5]

Finally, a few more remarks need to be made. One can argue that the oscillation of the trajectories in the local **1b*** minimum is an artifact of the MMVB method since this minimum does not exist at the MCSCF level. This is true and in reality we expect the system to oscillate in the **1o*** minimum before

Table 4. MMVB Dynamics Simulation for the Photochemical Ring-Opening Reaction of 8a,9-dihydrophenanthrene **1c**

trajectory[a]	ΔE_{ic}[b]	q (Å)[c]	t_{hop} (fs)[d]	t_{end} (fs)[e]	product
0	−27.8	1.564	176	710	**1c**
1	71.4	1.565	178	198	**1c**
2	40.9	1.583	292	480	**1c**
3	71.5	1.553	172	190	**1c**
4	77.8	1.586	211	440	**1c**
5	42.1	1.543	236	475	**1c**
6	55.9	1.467	249	462	**1c**
7	26.3	1.516	216	463	**1c**
8	69.0	1.556	124	165	**1c**
9	41.6	1.538	526	935	**1c**
10	6.4	1.586	154	467	**1c**

[a] Trajectory 0 was obtained without geometry and velocity sampling. Other trajectories have been sampled from the ground vibrational level of **1c**. [b] Energy difference in kcal/mol between the energy at which internal conversion occurs and the energy minimum at **1o***. [c] q is the bond length in Å of the C−C bond breaking/forming at the hop. [d] Time at the radiationless decay. [e] Total time of the trajectory.

overcoming the barrier (**TS***). Then, depending on vibrational motions, the system will either hit the $\mathbf{CI_1}$ crossing seam or relax to the **1c*** minimum where it decays at $\mathbf{CI_2}$ (see Figure 1). We also found another funnel on the open-ring side of the potential surface ($\mathbf{CI_3}$, Table 1, Figure S8). This crossing is of the same type as $\mathbf{CI_2}$ (prefulvene-like conical intersection). Trajectories sampled from the **1o** minimum were not found to reach this crossing seam (the MMVB barrier is over 20 kcal/mol, Table S2) and therefore, we do not expect this funnel to photostabilize the open-ring isomer.

Photochemical Ring-Opening Reaction of 8a,9-Dihydrophenanthrene. Lewis et al.[4] observed a complete reversion of **2c** to **2o** under 500 nm irradiation at 77 K, suggesting that the electrocyclic ring opening of singlet **2c** also occurs via a funnel with a small barrier. However, the results of our simulation on model system **1** (Table 4) shows that the ring-opening reaction does not take place on the covalent S_1 surface calculated with MMVB (and also MCSCF). Indeed, the minimum energy path from the Franck−Condon region of **1c** leads to the **1c*** minimum. The trajectories show that the system relaxes quickly in this minimum and then reaches the $\mathbf{CI_2}$ crossing seam, where it decays to the ground state in a closed-ring form to regenerate **1c**. Therefore, the ring-opening photoreaction takes place on a different potential energy surface, at least initially.

We must therefore assume that, after excitation of **1c** to the optically active ionic L_a state, decay to the covalent state does not take place immediately after irradiation, and the photoreaction begins on the L_a state. This is supported by MRPT2 results at the **1c** geometry: the ionic L_a state was found 8 kcal/mol below the covalent L_b state, in contrast to **1o**. The MRPT2 vertical excitation energy for the L_a state is calculated to be at 483 nm, close to the 500 nm experimental excitation, which gives us some confidence in this result. The L_a state cannot be described at the MMVB level, because of its ionic character, so we cannot model the dynamics on this surface. Similarly, our CASSCF/RASSCF calculations are inadequate to compute such a state accurately (they predict the S_1 state to be covalent), as dynamic electron correlation is essential. At present, we cannot optimize an S_0/S_1 crossing with MRPT2 for this system, so the details of the radiationless decay of **1c** remain uncertain.

Finally, the existence of the same conical intersections $\mathbf{CI_1}$ and $\mathbf{CI_2}$ in system **2** suggests similar mechanisms for the photoreactivity of 2-vinyl-1,3-terphenyl to the ones described above for 2-vinylbiphenyl. This was verified by the calculation of two trajectories simulating the photocyclization and photochemical ring-opening reaction. Again, the ring-opening reaction did not occur on the S_1 surface.

Conclusion

We present in this work a realistic mechanism for the photocyclization of 2-vinylbiphenyl and its derivatives. It is supported by extensive ab initio MCSCF calculations and MMVB dynamics simulations. We found a near-barrierless reaction pathway along the cyclization coordinate on the S_1 potential energy surface. Two distinct funnels for internal conversion to the ground state were located and lie close to the reaction path. Dynamics simulations show that they can easily be accessed during the cyclization process and are responsible for the formation of the closed-ring intermediate, which in turn forms the final photoproduct upon heating. Access to these two funnels leads to two different mechanisms: in the first one, the cyclization is nonadiabatic and the ring-closure is completed on S_0 after internal conversion; in the second, the cyclization is adiabatic and the ring-closure occurs exclusively on the S_1 surface before internal conversion to S_0. Moreover, the photochemical ring-opening reaction from the closed-ring intermediate was shown to be impossible on the S_1 surface and involves another electronic state initially. The mechanism for this process remains the subject of further studies.

Finally, Lewis et al.[37] recently observed that product formation occurs predominantly via 1,2-hydrogen shift, despite the fact that the calculated barrier for the 1,5-shift is predicted to be significantly lower than that for the 1,2-shift. The study of the hydrogen shift leading to the final product is outside the scope of this article. Nonetheless it is possible that this is a consequence of decay from a conical intersection funnel favoring the 1,2-shift, even though it is not the pathway on the ground-state surface with the lowest barrier.

Acknowledgment. This work has been supported by EPSRC UK (grant GR/S94704/01). We thank Professor Frederick D. Lewis for suggesting this study. We thank the EPSRC National Service for Computational Chemistry Software (www.nsccs.ac.uk) for enabling us to run the MOLPRO calculations.

Supporting Information Available: Cartesian coordinates for optimized RASSCF structures. Table S1 for RASSCF energetics obtained with 4-31G basis set. Tables S2 and S3 for MMVB energetics of 2-vinylbiphenyl and 2-vinyl-1,3-terphenyl, respectively. Figure S1 for comparison of CASSCF and RASSCF optimized structures. Figure S2 for MMVB potential energy profile of 2-vinylbiphenyl. Figure S3 for the main MMVB optimized structures. Figure S4 for local minima and transition states found with MMVB on S_1 surface of 2-vinylbiphenyl. Figure S5 for MMVB potential energy profile of 2-vinyl-1,3-terphenyl. Figure S6 for local minima and transition states found with MMVB on S_1 surface of 2-vinyl-1,3-terphenyl. Figure S7 for the transition vectors of the different transition states. Figure S8 for structure of $\mathbf{CI_3}$. Complete refs 31 and 32. This material is available free of charge via the Internet at http://pubs.acs.org.

JA062901Z

(37) Lewis, F. D.; Sajimon, M. C.; Zuo, X.; Rubin, M.; Gevorgyan, V. *J. Org. Chem.* **2005**, *70*, 10447−10452.